Journal of Molecular Structure 1293 (2023) 136189

Contents lists available at ScienceDirect

Journal of Molecular Structure

journal homepage: www.elsevier.com/locate/molstr

Environmentally-friendly synthesis, structural determination and antimicrobial activity of new class of spiropyrrolidine embedded with indenoquinoxaline and chromanone heterocyclic units

Natarajan Arumugam [a,*], Saied M. Soliman [b], Vijayan Viswanathan [c], Abdulrahman I. Almansour [a], Raju Suresh Kumar [a], Sakkarapalayam M. Mahalingam [d,*], Bellie Sundaram Krishnamoorthy [e], Necmi Dege [f], Ponmurugan Karuppiah [g], Karthikeyan Perumal [h]

[a] Department of Chemistry, College of Science, King Saud University, P.O. Box 2455, Riyadh 11451, Saudi Arabia
[b] Department of Chemistry, Faculty of Science, Alexandria University, P.O. Box 426, Ibrahimia, Alexandria 21321, Egypt
[c] Department of Biophysics, All India Institute of Medical Sciences, New Delhi 110029, India
[d] Department of Chemistry, PSG College of Arts and Science and PSG Institute of Advanced Studies, Coimbatore, Tamil Nadu 641014 India
[e] Department of Chemistry (UA), PSG College of Arts and Science, Coimbatore-14, Tamil Nadu, India
[f] Department of Physics, Faculty of Arts and Sciences, Ondokuz Mayıs University, Samsun 55139, Turkey
[g] Department of Botany and Microbiology College of Science, King Saud University, P.O. Box No.2455, Riyadh 11451, Saudi Arabia
[h] Department of Chemistry and Biochemistry, The Ohio State University, 151W. Woodruff Ave, Columbus, OH 43210, USA

ARTICLE INFO

Keywords:
Spiropyrrolidine
[3+2]-cycloaddition
Single crystal X-ray structure study
Computational study
Hirshfeld analysis
Antimicrobial activity

ABSTRACT

A regio- and stereoselective synthesis of hitherto unexplored novel class of dispiropyrrolidine embedded with indenoquinoxaline and chromanone hybrid heterocycle has been achieved employing an eco-friendly ionic liquid assisted multicomponent 1,3-dipolar cycloaddition cascade protocol. The dipolarophile, 3-(4-methoxybenzylidene)chroman-4-one reacts with non-stabilized 1,3-dipole component derived from indenoquinoxalinone and L-phenylalanine through decarboxylative cascade reaction pathway affording (2′S,4′S)-5′-benzyl-4′-(4-methoxyphenyl)dispiro[chromane-3,3′-pyrrolidine-2′,11′′-indeno[1,2-*b*]quinoxalin]-4-one (**6**) as the final product. The structure of **6** was confirmed through NMR and mass spectroscopic analyses. Further, stereochemistry of the spirocompound was undoubtedly determined through single crystal XRD analysis. In the crystal structure, the O…H and N…H interactions are the most common contacts and also have great importance in molecular packing. In addition, the C…H contacts are also important in the studied crystal structure. DFT and NBO calculations were performed on this system in order to discuss its electronic and reactivity parameters. The calculated dipole moment value is 2.9238 Debye indicating a polar compound. Compound **6** was assayed for antimicrobial efficacy and found to have potential activity against eight tested microbial pathogens. Among them, *E. coli* ML_KSUB22 and *C. albicans* ML_KSUF05 were found to be highly susceptible than the other pathogens.

1. Introduction

Synthesis of structurally intriguing hybrid heterocyclic architectures is very attractive to organic chemists as they have been found in a significant number of pharmaceutically and biologically relevant compounds. Among them, spiroanalogues are privileged class of pharmacophore in drug discovery as they have an exclusive three-dimensional structural feature which can be likely to interact better with target enzyme than other planar aromatic ring systems. Heterocycles comprising spiropyrrolidine have particularly emerged as an interesting synthetic compound in medicinal chemistry since spiropyrrolidine heterocyclic moiety commonly existing as the active motif in many biologically relevant alkaloids and other pharmaceutically important synthetic analogues. For example, spirotryprostatin,

* Corresponding authors.
E-mail addresses: anatarajan@ksu.edu.sa (N. Arumugam), mahalingam@psgcas.ac.in (S.M. Mahalingam).

https://doi.org/10.1016/j.molstruc.2023.136189
Received 20 March 2023; Received in revised form 19 June 2023; Accepted 10 July 2023
Available online 11 July 2023
0022-2860/© 2023 Elsevier B.V. All rights reserved.

horsfiline, elacomine and strychnofoline have shown multifarious biological activities including inhibition of microtubule assembly [1], G2/Mphase inhibitory activity at mammalian cell cycle [2], modulation of the function of muscarinic serotonin receptors [3], anti-proliferative activity against brain cancer cell lines, malignant glioma GAMG [4], anti-inflammatory, anti-mycobacterial [5], antimicrobial [6], analgesic [7], local anesthetic [8], and acetylcholine esterase inhibitory activities [9].

Chromanone is another important class of heterocyclic moiety found in natural and synthetic products such as polyphenols and taxifolin which have shown promising inhibitory activity against microbial infection, inflammation, oxidative stress, malignancy, liver disease and cardiovascular disease. In addition, chromanone derivatives have shown multifarious biological activity including protein kinase and tyrosine inhibitors, anticancer [10–13], neuroprotective [14], anti-vascular, antidiabetic, anti-leishmanial, spasmolytic, analgesic, anticoagulant, estrogenic inhibitor, anti-AIDS [15–17], antimicrobial [18,19], anti-fungal [20] antioxidant activity [21], interleukin-5 inhibitory activity effect [22] and as anti-proliferative agents [23].

Multicomponent reaction (MCR) is one of protuberant place of synthetic strategy for the preparation of various heterocycles including spiroanalogues, which offers a rapid and powerful synthetic strategy for the construction of a wide variety of complex heterocycles of biological importance with high complexity and diversity [24,25]. In addition, MCR has great advantages in terms of convergence and atom economy with minimum number of preparation and purification steps which in turn results in an eco-friendly green protocol. In this context, the interest in ionic liquids as environmentally benign solvents make them a good choice for diverse chemical reactions because of their low vapor pressure and extremely high thermal stability, good solvating ability and ease of recyclability.

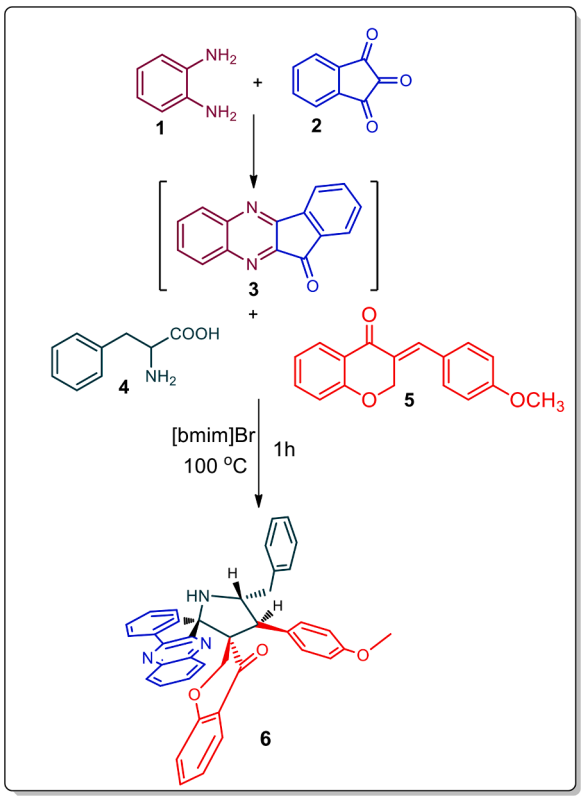
In view of the important biological activities mentioned above, we postulate that compounds embedding spiropyrrolidine with indenoquinoxaline and chromanone into a single molecule would be of great interest in pharmaceutical chemistry. Furthermore, the integration of the chromanone moiety into spirocompounds has often led to rise of the biological activity of the compounds. With the above facts in mind, herein we report a facile access to spiropyrrolidine fused chromanone heterocycles via a single pot protocol employing 1,3-dipolar cycloaddition strategy. In the present study synthesis and structural determination of a new class of spiropyrrolidine embedded chromanones were described by single crystal XRD, Hirshfeld surface analysis and DFT studies. In addition, the spirocompound was evaluated for its antimicrobial activity against eight common microbial pathogens.

2. Material and methods

2.1. Synthesis of spirocompound,6

A mixture of trikeone **1** (1 mmol), aryldiamine **2** (1 mmol), L-phenylalanine **3** followed by (E)-3-(4-methoxybenzylidene) chroman-4-one, **5** (1 mmol) were heated to 100 °C in [Bmim]Br (3 ml) for 1 h. The reaction mixture was diluted with EtOAc (2 × 5 mL) after absence of starting material was verified by TLC analysis and EtOAc was extracted and concentrated under reduced temperature. Finally, the product is washed with Et_2O and filtered to afford pure product in good yields. The single crystals of the compound were obtained by recrystallization from Ethyl acetate.

^{1}H NMR ($CDCl_3$, 500 MHz): δ_H 2.87–2.91 (dd, J = 14.00, 8.00 Hz), 3.14–3.17 (dd, J = 14.0, 3.0 Hz), 3.31 (d, J = 12.0 Hz, 1H), 3.78 (s, 3H), 4.62–4.66 (m, 1H), 5.15–5.19 (m, 1H), 6.12 (d, J = 8.0 Hz, ArH, 1H), 6.90–6.92 (m, ArH, 2H), 6.97–7.00 (m, ArH, 1H), 7.10–7.25 (m, ArH, 9H), 7.44–7.46 (m, ArH, 1H), 7.68–7.73 (m, ArH, 3H), 8.07–8.08 (m, ArH, 1H), 8.21–8.23 (m, ArH, 1H); ^{13}C NMR ($CDCl_3$, 125 MHz): δ_C 39.7, 51.2, 55.3, 61.5, 62.4, 71.9, 114.2, 116.6, 120.8, 121.0, 121.5, 126.4, 127.7, 128.5, 129.2, 129.3, 129.4, 129.6, 131.0, 135.1, 136.7, 138.8, 140.7, 142.2, 147.0, 153.8, 159.0, 160.2, 165.2, 192.8. Mass: m/z 601 (M^+). Anal. Calcd. For $C_{40}H_{31}N_3O_3$: C, 79.85; H, 5.19; N, 6.98%; Found: C, 79.97; H, 5.30; N, 7.05%.



Scheme 1. Synthesis of structurally diverse dispiroindenopyrrolidine tethered chromanone **6**.

2.2. X-ray analysis

XRD intensity data were collected at 293 K on a Bruker D8 VENTURE single crystal X-ray diffractometer equipped with graphite monochromatic Mo$K\alpha$ radiation (λ=0.71073 Å) and PHOTON 100 CMOS detector. The crystal of dimension 0.100×0.150×0.150 mm^3 for the title compound was attached to a glass fiber using cyanoacrylate adhesive. The unit cell parameters were analyzed from 36 frames measured (0.5° phi-scan) from three different crystallographic zones employing the difference vector method. The intensity data were collected with an average four-fold redundancy per reflection and optimal resolution (0.75 Å).

2.3. Hirshfeld surface analysis

The topology analyses were carried out by Crystal Explorer 17.5 program [26].

2.4. Computational methods

All DFT calculations were carried out by Gaussian 09 software package [27] using B3LYP/6-31G(d,p) method. Natural charges were calculated bonds were calculated using NBO 3.1 program as implemented in the Gaussian 09 W package [28].

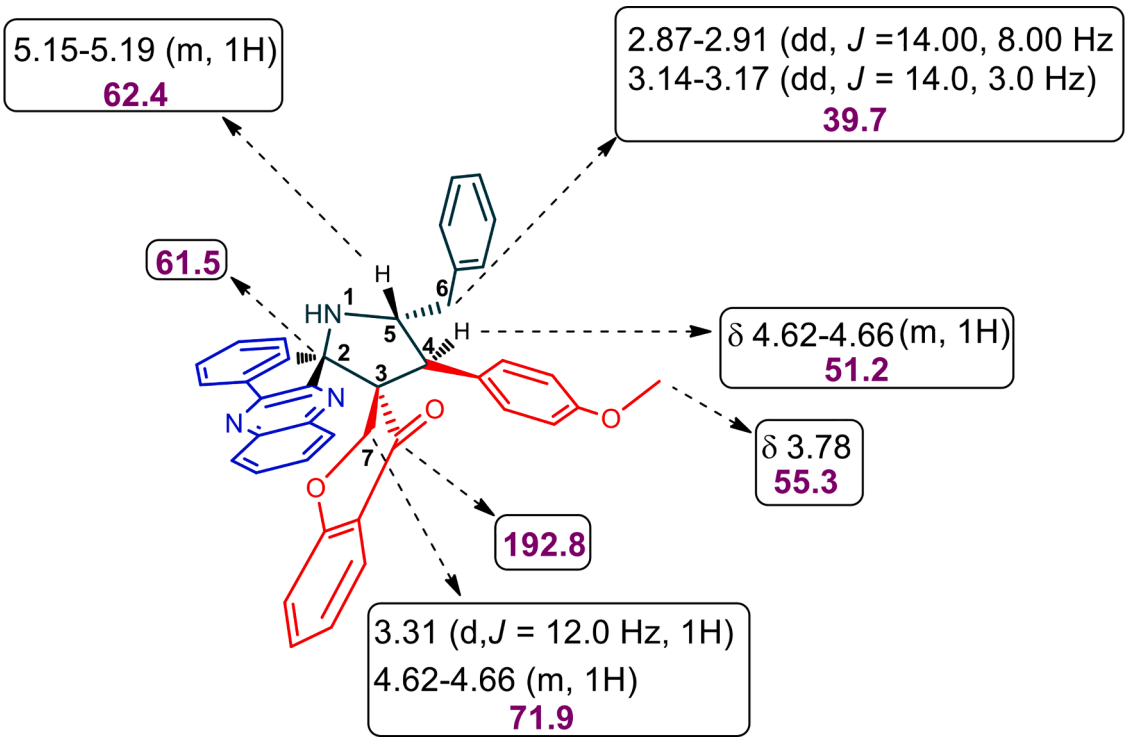


Fig. 1. Chemical shifts of **6**.

3. Results and discussion

3.1. Synthesis and characterizations

The highly functionalized 3-(4-methoxybenzylidene)chroman-4-one **5** was synthesized from chromanone and 4-methoxy benzaldehyde in the presence of HCl according to the protocol described in the literature [29]. With the dipolarophile **5** in hand, we began our investigation on the [3 + 2]-cycloaddition cascade protocol of 3-(4-methoxybenzylidene) chroman-4-one **5** with the 1,3-dipole generated in situ from indenoquinoxalinone and α-amino acid upon heating to 100 °C in [Bmim]Br, which led to the formation of chromanone integrated spiroindenopyrrolidine hybrid heterocycle **6** as a single cycloadduct in excellent yield (92%) after 1 h (Scheme 1). Initially, the solvent optimization was examined with an equimolar mixture of **1, 2, 4** and **5** in various organic solvents namely, CH_3OH, EtOH, CH_3CN, 1,4-dioxane including mixture of solvents *viz*. acetonitrile:1,4-dioxane (1:1 v/v) afforded 68, 62, 55, 58 and 64%. Ultimately, the cycloaddition cascade protocol was performed with ionic liquid, [Bmim]Br at 100 °C for 1 h and the disappearance of starting materials and the formation of the product was confirmed by TLC. The reaction mixture was diluted with EtOAc and H_2O and then the ethyl acetate was concentrated under reduced temperature. Finally, the residue was washed with Et_2O to give the pure cycloadduct in 92% yield. In a previous study, we reported the synthesis, structural elucidation, computational determination and biological potential of spirooxindolopyrrolidine heterocycles employing three/four component cycloaddition reaction [30,31], whereas in the present study synthesis of spiropyrrolidine with indenoquinoxaline and chromanone has been accomplished by a four-component cycloaddition strategy under green chemistry protocol. In addition, its structural determination and antimicrobial activity was also established. To the best of our knowledge this is the first report on the synthesis of a complex molecule with the combination of spiropyrrolidine, indenoquinoxaline and chromanone heterocyclic units.

The structure of synthesized spiroindenopyrrolidine integrated chromanone was determined by spectroscopic analysis (Fig. 1). The ^1H

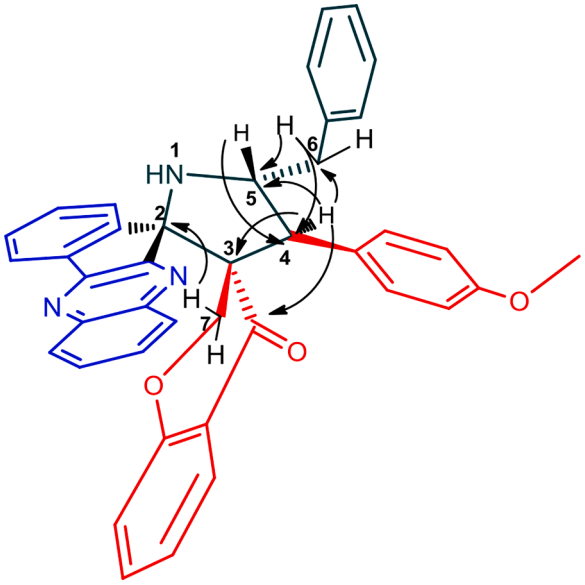
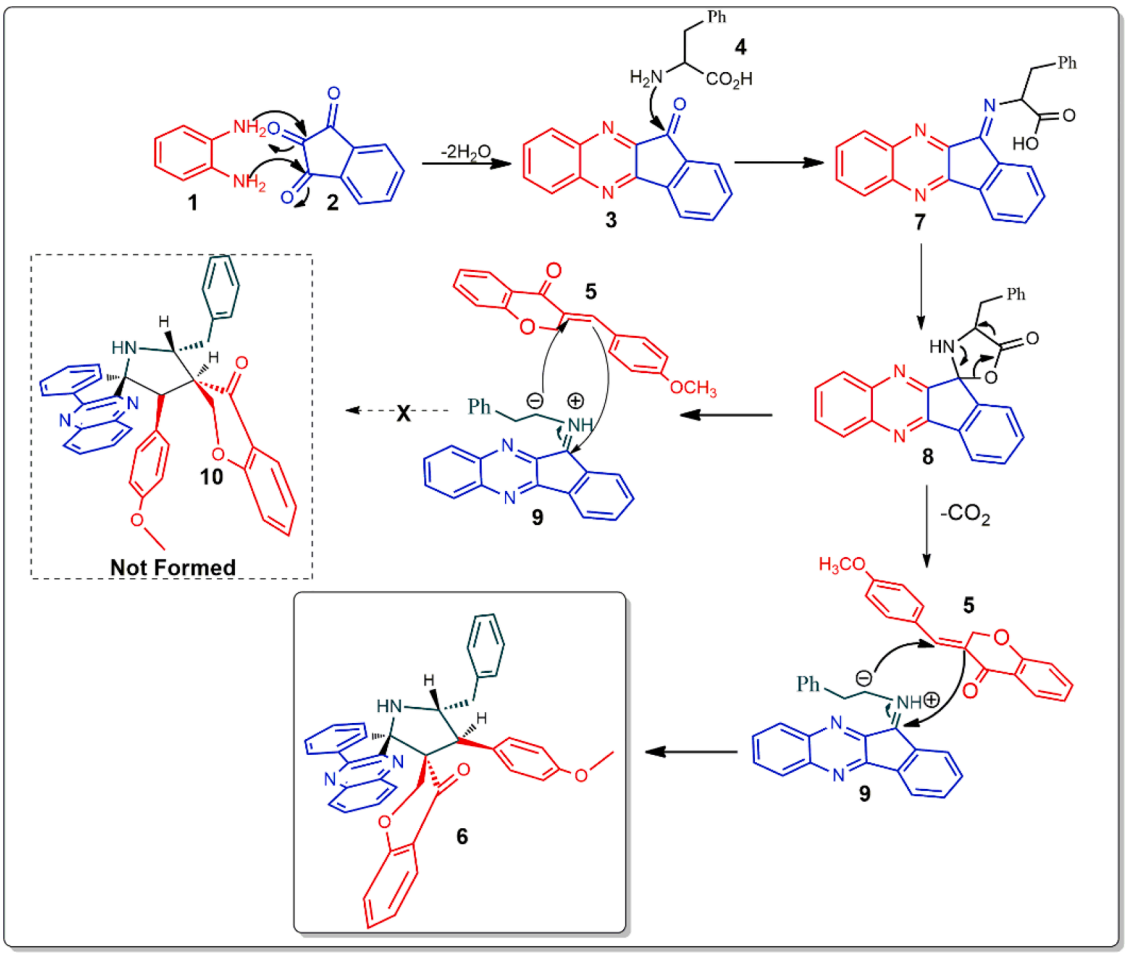


Fig. 2. HMBCs of **6**.

NMR spectrum of **6** has a multiplet at δ 5.15–5.19 ppm ascribable to H-5 hydrogen of the pyrrolidine ring which showed (i) H,H—COZY correlation at δ 2.87–2.91 and 3.14–3.17 ppm was related to H-6 hydrogen (ii) HMBCs (Fig. 2) with C-4 at δ 51.2 ppm. H-6 hydrogens showed (i) HMBCs with C-4 and C-5 at δ 51.2 and 62.4 ppm, respectively (ii) H, H—COZY correlation to each other. A multiplet at δ 4.62–4.66 was assigned to benzylic hydrogen (H-4) of pyrrolidine ring which showed HMBCs with C-6 (benzylic carbon), C-5, C-7 and chromanone carbonyl carbon at δ 39.7, 62.4, 71.9 and 192.8 ppm. The chromanone methylene hydrogens (H-7) showed as multiplet at δ 4.62–4.66 and a doublet at δ 3.31 (J = 12.0 Hz). It is pertinent to note that H-4 and H-7 hydrogens are merged together in same region at δ 4.62–4.66 as discussed early. H-7



Scheme 2. A feasible mechanism for the formation of spiroyrrolidine, **6**.

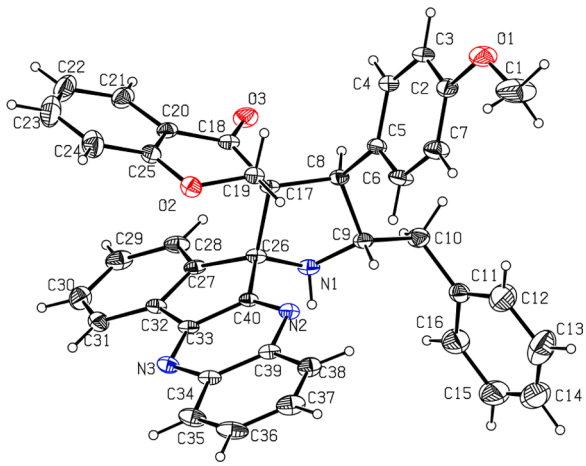


Fig. 3. X-ray structure with atom labeling and displacement ellipsoids drawned at 30%.

hydrogen showed HMBCs with C-2 (spirocarbon) at 61.5 ppm. Further, the spiro, methyl and methine carbons were assigned with no doubt through DEPT-135 spectrum. Further, the regio and stereochemistry of the compounds was unambiguously determined through single crystal X-ray diffraction analysis [32].

A persuasive mechanism for the creation of the dispiropyrrolidine integrated chromanone **6** is described in Scheme 2. Initially, the reaction of ninhydrin **2** and phenylenediamine **1** generates indenoquinoxalinone **3** intermediate by spontaneous elimination of H_2O which further reacts with L-phenylalanine **4** producing the in situ ylide **9** through the intermediates, iminium ion **7** and oxazolidinone **8**. Consequently, the in situ ylide **9** was added to the Carbon-Carbon bond of 3-(4-methoxybenzylidene)chroman-4-one **5** furnishing the expected cycloadduct **6** in preference to other possible regioisomeric product **10**.

3.2. X-ray diffraction studies

The titled compound was crystallized in the monoclinic $P2_1$ space group and the unit cell parameters are $a = 13.485(18)$ Å, $b = 11.0322(14)$ Å, $c = 21.808(3)$ Å, $\beta = 104.878(4)$ ° and $Z = 4$. The three-dimensional molecular structure of the compound was determined by X-ray crystallography. The molecular structure and the numbering scheme of the titled compound are illustrated in Fig. 3 with displacement ellipsoids drown at 30% probability level. The pyrrolidine ring is fused with the indeno quinoxaline, chroman-4-one, toluene and phenyl ring moieties in the crystal structure. The pyrrolidine ring adopts a twisted conformation in most of molecules [33–39] and have envelope conformation in few of compound as observed in previously literature reports [38–40]. In the titled crystal structure, the pyrrolidine ring (N1/C8/C9/C17/C26) adopt a twisted conformation on N1—C9 bond with puckering parameters [41] q2 = 0.418(4) Å, ϕ2 = 10.2(5) °. In the chroman-4-one ring system, the chroman ring (O2/C17-C20/C25) adopts a twisted conformation on C17-C19 bond with puckering parameters $q = 0.488(4)$ Å, $\phi = 76.1(5)$ ° and $\theta = 52.9(2)$ °. In the crystal structure, the pyrrolidine ring (N1/C8/C9/C17/C26) is fused with the indeno quinoxaline ring (N2/N3/C26-C40) and chroman-4-one ring systems (O2/C17-C25) and these two ring systems are almost

Table 1
The crystal data and structure refinement details for the title compound.

Parameters	Values
Empirical formula	C_{40} H_{31} N_3 O_3
Formula weight	601.68
Temperature	293(2) K
Wavelength	0.71073 Å
Crystal system	Monoclinic
Space group	P 2_1/n
Unit cell dimensions	a = 13.4850(18) Å α = 90 ° b = 11.0322(14) Å β = 104.878(4) °. c = 21.808(3) Å γ = 90 °
Volume	3135.6(7) Å^3
Z, Calculated density	4, 1.275 Mg/m^3
Absorption coefficient	0.081 mm^{-1}
F(000)	1264
Crystal size	100×150×150 mm^3
Theta range for data collection	2.673 to 26.000 °
Limiting indices	$-14 \leq h \leq 16$ $-13 \leq k \leq 13$ $-26 \leq l \leq 26$
Reflections collected / unique	35,984 / 6126 [$R_{(int)}$ = 0.1024]
Completeness to theta = 25.242	99.60%
Absorption correction	Semi-empirical from equivalents
Refinement method	Full-matrix least-squares on F^2
Data / restraints / parameters	6126/0/420
Goodness-of-fit on F^2	1.122
Final R indices [I>2sigma(I)]	R_1 = 0.0906, wR_2 = 0.1615
R indices (all data)	R_1 = 0.1739, wR_2 = 0.1913
Largest diff. peak and hole	0.229 and −0.224 e. Å^{-3}

Table 2
Hydrogen bond geometry for the title compound [Å and °].

D—H•••A	D—H(Å)	H•••A(Å)	D•••A(Å)	D—H•••A[°]
N1—H1•••N3$^{(i)}$	0.83(4)	2.36(4)	3.147(5)	159.4
C8—H8•••O3	0.98	2.32	2.844(4)	113
C9—H9•••N2	0.98	2.62	3.244(5)	122
C19—H19A•••O1$^{(ii)}$	0.97	2.48	3.399(5)	159
C19—H19B•••N2	0.97	2.41	3.049(5)	123
C1—H1C•••Cg1$^{(ii)}$	0.97	2.89	3.815(1)	161
C23—H23•••Cg2$^{(iii)}$	0.97	2.92	3.684(2)	141

Symmetry code: (i) 1-x, 1-y, 1-z; (ii) 2-x, -y, 1-z; (iii) $-1/2 + x$, 1/2-y, $-1/2 + z$.

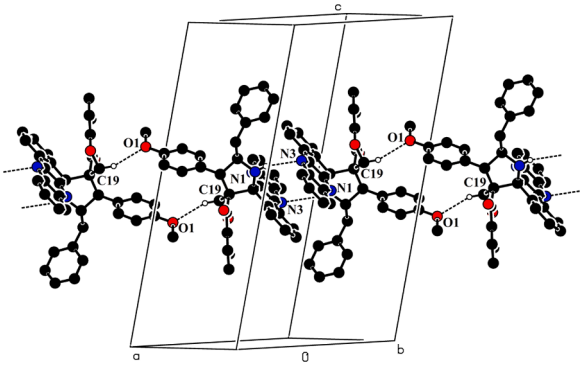


Fig. 4. Crystal packing of the title compound via the hydrogen bonds that produce inversion dimmers with $R_2^2(12)$ and $R_2^2(18)$ ring motifs. For the sake of clarity, H atoms not connected by hydrogen bonds are left out.

orthogonal by 88.26(16) ° and 90.0(18) ° with the pyrrolidine ring, respectively. The anisole ring (O1/C1-C7) and toluene ring (C10-C16) moieties make a dihedral angle of 76.7(2) ° and 53.6(2) ° with the pyrrolidine ring, respectively (Table 1).

Intermolecular interactions between N—H•••N and C—H•••O, C—H•••π and π•••π hydrogen bonds as well as intramolecular C—H•••O and C—H•••N bonds help to stabilize the crystal structure

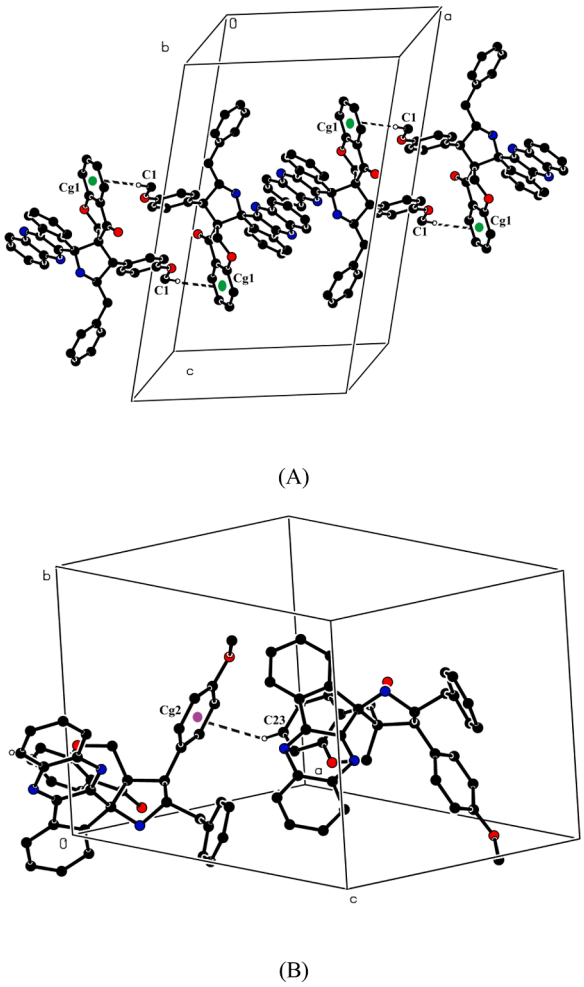


Fig. 5. The C—H•••π interactions in the title compound. H atoms not involved in hydrogen bonds are omitted for clarity.

(Table 2). Fig. 4 shows the molecular interaction between the N1—H1•••N3, C19—H19A•••O1 cyclic centrosymmetric inversion dimmers with an $R_2^2(12)$ and $R_2^2(18)$ ring motifs are produced via these two-hydrogen bonding. These two intermolecular hydrogen bond interactions are responsible for the formation of a *C(9)* and *C(7) zigzag* infinity chain that extends along the [1 1 0] plane. C1—H1C•••π (Cg1) and C23—H23•••π (Cg2) are weak intermolecular interactions between the centroid of the six-membered cyclic chroman ring (Cg1) and the six-membered anisole ring (Cg2) as shown in Fig. 5A and 5B. In the crystal packing, the molecules are stacked in layers held together by π—π interactions are also observed in the crystal structure.

3.3. Hirshfeld analysis

Analysis of molecules' packing in the crystal structure has a great importance for determining the intermolecular interactions occurred in the crystalline materials. In this regard, we employed Hirshfeld surface analysis of molecular packing for this task. The d_{norm} map is characterized by three distinct coloured regions which are the red (shorter), white (equal) and blue (longer) regions relative to the vdWs radii sum of the interacting atoms. The d_{norm} map for the studied crystal is shown in Fig. 6. All short contacts which control the molecular packing of the studied crystal are labelled in yellow color (**A** to **C**) in this figure. It is clear that the O…H and N…H interactions are common and have great importance in the molecular packing. On the other hand, the molecular packing of compound **6** is further controlled by some C…H contacts. These intermolecular interactions are shorter than the vdWs radii sum of

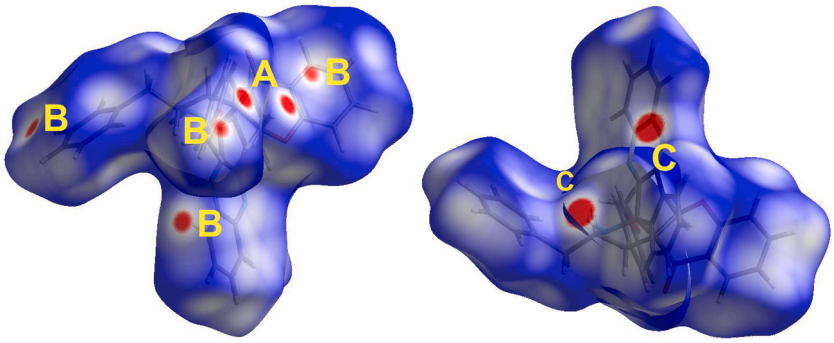


Fig. 6. Hirshfeld d_{norm} surfaces for **6**. **A**: O…H, **B**: C…H and **C**: N…H.

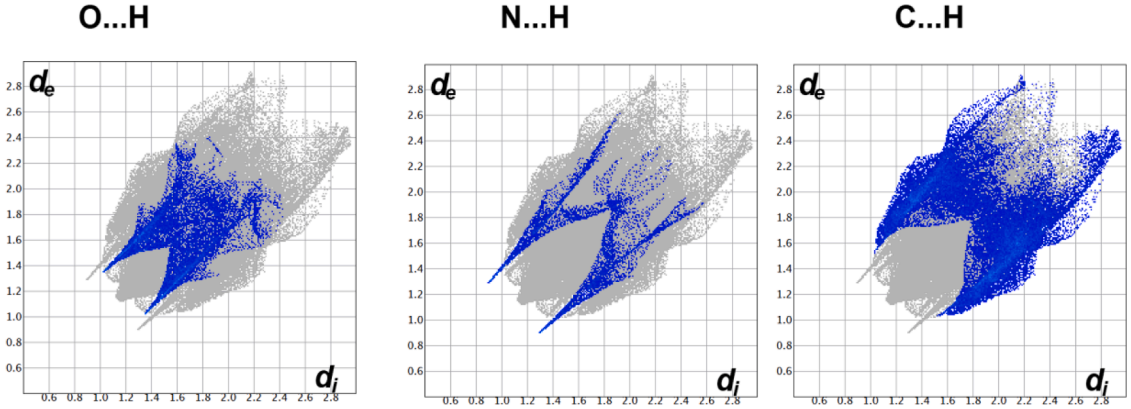


Fig. 7. Fingerprint plots of the important O…H, N…H, and C…H interactions in **6**.

Table 3
Possible intermolecular contacts and their percentages in **6**.

Contact	6
C…O	0.2
O…H	8.7
N…H	3.8
C…N	0.8
C…C	4.7
C…H	21.5
H…H	60.3

the interacting atoms and hence appeared as red regions in the corresponding d_{norm} maps.

The decomposed fingerprint plots of the O…H, N…H, and C…H interactions appeared as sharp spikes which further indicate that these interactions occurred at short distances (Fig. 7). Also, decomposition of the fingerprint plots gave a quantitative summary for all intermolecular interactions in the crystal of **6**. Summary of all contacts and their percentages in the studied system are presented Table 3. The most dominant contacts are the H…H, C…H and O…H interactions. The percentage contribution of the H…H interactions is 60.3%. The respective values for the C…H and O…H contacts are 21.5% and 8.7%, respectively. Although the%C…C interactions in compound **6** is 4.7% but the C…C contacts occurred at longer distances than twice the vdWs radii of carbon atom indicating insignificant π-π stacking interactions. This fact is further revealed by the absence of the characteristic red regions related to the C…C interaction in the d_{norm} map. The curvedness and shape index maps shown in Fig. S11 (Supplementary data) revealed the same conclusion.

3.4. DFT studies

The structure of **6** is optimized using DFT/B3LYP calculations. The optimized geometry of each compound **6** is matching well with the experimental X-ray structure where little differences might be attributed to the phase differences between the optimized geometry and the experimental one (Fig. 8). In addition, Fig. 9 shows plotting of the calculated bond distances against the experimental values gave good straight-line correlation with high correlation coefficient (R2= 0.9967).

The different electronic and reactivity parameters are calculated at the optimized structure of the studied system. The natural atomic charges at the different atomic sites are listed in **Table S6** (Supplementary data). The oxygen and nitrogen atoms have high negative charge. Also, all carbon atoms except those attached to the N or O atoms are negatively charged. As clearly seen from the molecular electrostatic potential (MEP) map, there are red colored regions close to these atomic sites (Fig. 10). These regions represent the atomic sites with the highest negative charge density. In contrast, the most positive atomic sites are the hydrogen atoms specially the NH proton and the C-atoms bonded to N or O atoms. As a result of these differently charged regions, compound **6** has significant polarity. The calculated dipole moment value is 2.9238 Debye.

In the same figure the frontier molecular orbitals (HOMO and LUMO) are presented. Both molecular orbitals are delocalized mainly over the π-system of the studied molecule. Hence, the HOMO–LUMO excitation could be described as π-π transition. The energies of these molecular orbitals are given in Table 4. Based on these results, the HOMO–LUMO energy gap is calculated to be 3.832 eV. In addition, the energies of the frontier molecular orbitals are used to calculate the different reactivity parameters such as the ionization potential (I=-E_{HOMO}), electron affinity (A= -E_{LUMO}), chemical potential ($\mu = -(I + A)/2$), hardness ($\eta = (I-A)/2$) as well as electrophilicity index ($\omega = \mu^2/2\eta$) reactivity indices [42–49]

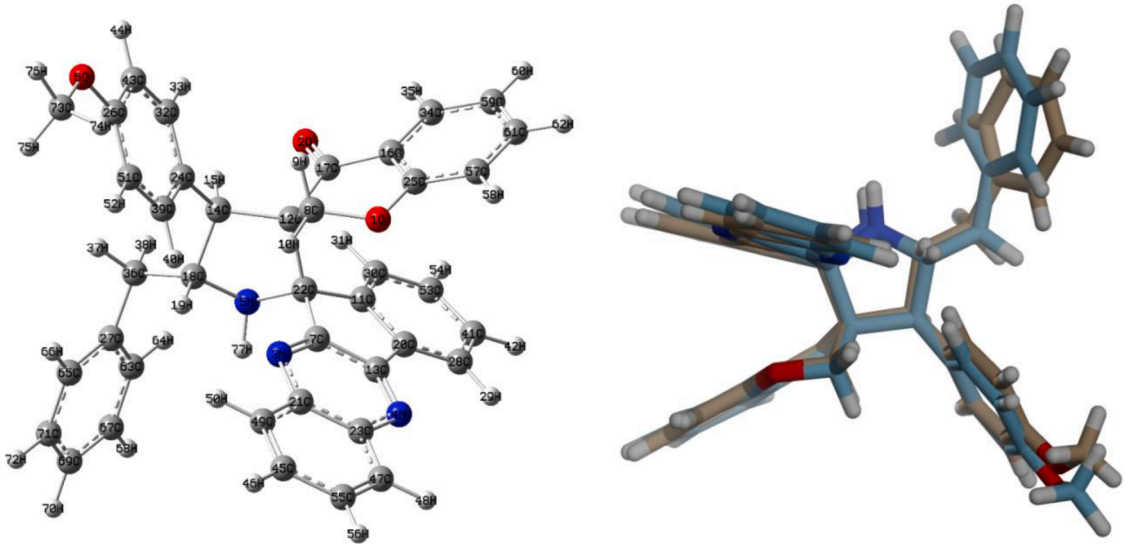


Fig. 8. Optimized structure (left) and structure matching between the calculated and experimental one (right) for **6**.

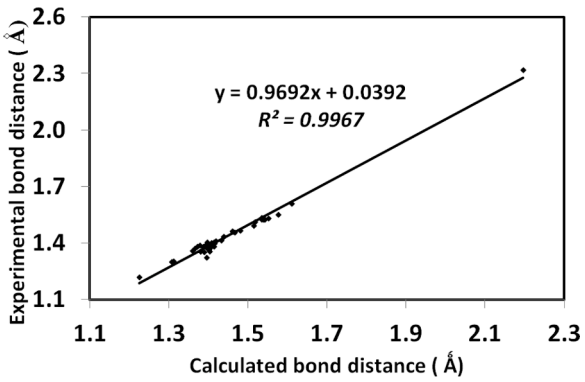


Fig. 9. The straight-line correlation between the calculated and experimental bond distances. List of bond distances and angles are depicted in Tables S4 and S5 (Supplementary data).

(Table 4). These parameters have important rule in the biomolecular reactivity of the studied system.

3.5. Antimicrobial activity

The antimicrobial activity of compound **6** was evaluated using agar well diffusion method on various microbial pathogens. The antimicrobial results are shown in Table S7 and Fig. 11 and were given by zone of inhibition (ZOI) in mm values. Compound **6** exhibited significant antimicrobial activities against the tested bacterial and fungal pathogens compared to the standard antibiotics, such as streptomycin and amphotericin B, respectively. Compound **6** displayed significant activity against bacterial pathogens *viz*., *E. coli* ML_KSUB22 (21.00 ±0.50 mm) followed by *S. aureus* ML_KSUB07 (19.00±0.35 mm) at 100 mg/mL, which is comparable activity to the standard drug, streptomycin (20.50±0.50) while compound **6** displayed good to moderate activity against E. *coli* ATCC25922 (19.00±0.30), *P. aeruginosa* ML_KSUB101 (18.50±0.20), *A. baumannii* ML_KSUB55 (17.00±0.15), respectively. Similarly, compound **6** showed good to moderate antifungal potential against tested fungal pathogens. Compound **6** displayed potent

Table 4
The calculated electronic parameters of **6**.

Parameter	6
E_{HOMO}	−5.8214
E_{LUMO}	−1.9892
Dipole moment	2.9238
I	5.8214
A	1.9892
η	3.8322
μ	−3.9053
ω	1.9899

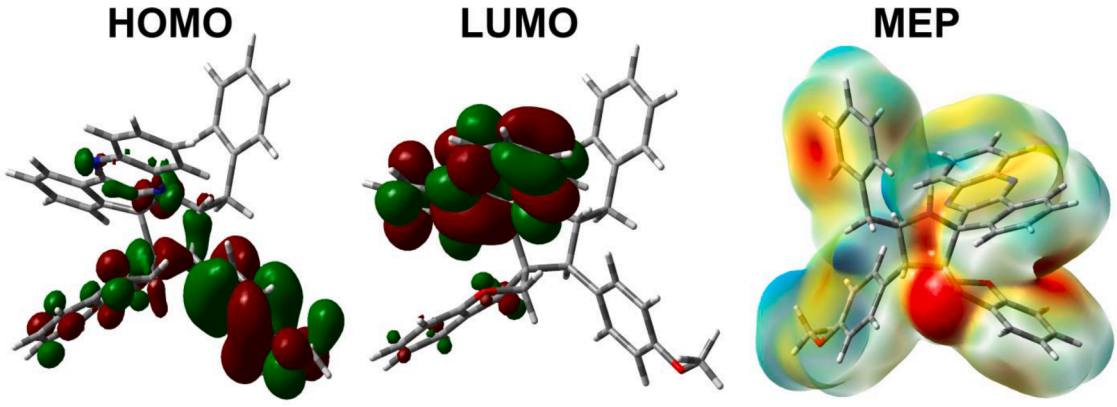


Fig. 10. The MEP, HOMO and LUMO of **6**.

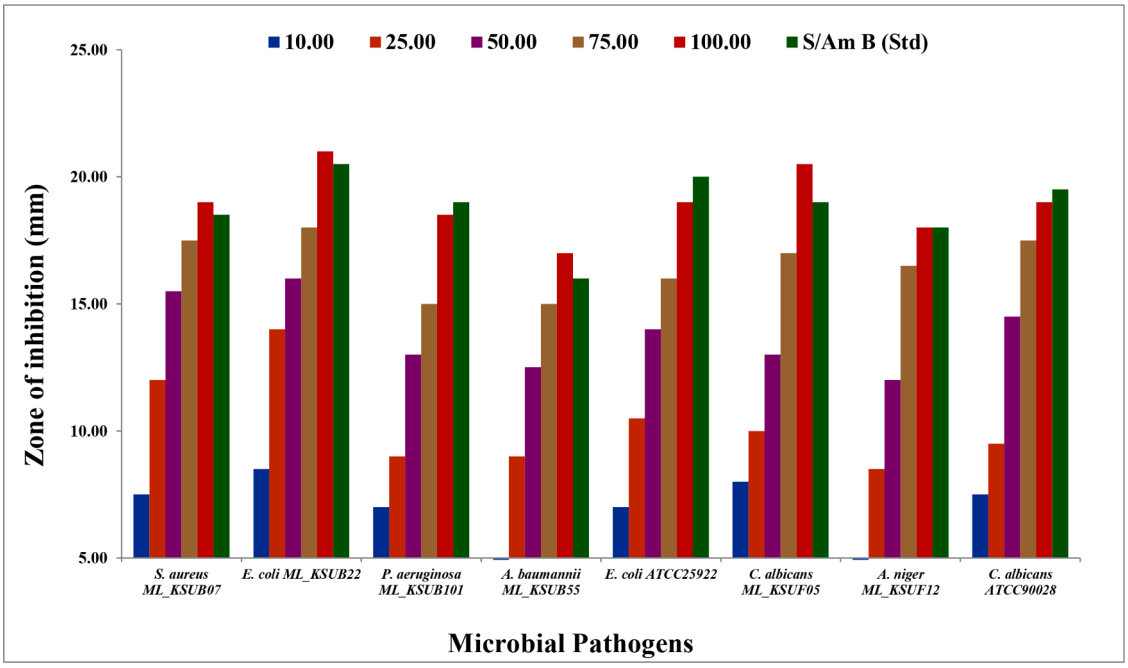


Fig. 11. Antimicrobial activity of compound **6** towards bacterial and fungal pathogens.

antifungal activity against *C. albicans* ATCC90028 (20.50±0.10 mm) which has comparable activity to the reference standard, amphotericin B (19.00±1.20 mm) while compound **6** displayed good to moderate activity with other fungal pathogens *viz*., *C. albicans* ML_KSUF05 (19.00 ±0.40), *A. niger* ML_KSUF12 (18.00±0.25) at 100 mg/mL. The study revealed that compound **6** exhibits potential antimicrobial activity against tested common microbial pathogens and anticipated to be a therapeutically important molecule in biomedical fields in the future.

4. Conclusion

In conclusion, a new class of spiropyrroloquinoxaline integrated chromanone heterocycle has been synthesized in excellent yield employing [Bmim]Br accelerated one-pot four component cascade reaction protocol involving a key intermolecular 1,3-dipolar cycloaddition strategy. 1,3-Dipole component, azomethine ylide derived from quinoxalinone and L-phenylalanine reacts with 3-(4-methoxybenzylidene) chroman-4-one affording the structurally interesting spirocycloadduct. The supramolecular structure of the spirocompound is determined by Hirshfeld calculations. The optimized molecular structures of studied system are calculated and its electronic properties such as dipole moment, HOMO, LUMO and the derived reactivity descriptors were discussed. In addition, the compound **6** displayed significant antimicrobial activity against tested microbial pathogens which is comparable activity with respect to the standard drug.

CRediT authorship contribution statement

Natarajan Arumugam: Conceptualization, Methodology, Formal analysis, Investigation, Resources, Writing – original draft, Supervision, Project administration, Funding acquisition. **Saied M. Soliman:** Software, Writing – original draft, Writing – review & editing. **Vijayan Viswanathan:** Software, Writing – original draft, Writing – review & editing. **Abdulrahman I. Almansour:** Methodology, Resources, Funding acquisition, Supervision, Project administration. **Raju Suresh Kumar:** Writing – original draft. **Sakkarapalayam M. Mahalingam:** . **Bellie Sundaram Krishnamoorthy:** . **Necmi Dege:** Formal analysis, Investigation. **Ponmurugan Karuppiah:** . **Karthikeyan Perumal:** Formal analysis, Investigation.

Declaration of Competing Interest

There is no conflict of interest

Data availability

Data will be made available on request.

Acknowledgment

The project was funded by Researchers Supporting Project Number (RSP2023R143), King Saud University, Riyadh, Saudi Arabia. The authors acknowledge to Scientific and Technological Research Application and Research Center, Sinop University, Turkey, for the use of the Bruker D8 QUEST diffractometer.

Supplementary materials

Supplementary material associated with this article can be found, in the online version, at doi:10.1016/j.molstruc.2023.136189.

Reference

[1] M.M. Khafagy, A.H.F.A. El-Wahas, F.A. Eid, A.M. El-Agrody, Synthesis of halogen derivatives of benzo[h]chromene and benzo[a]anthracene with promising antimicrobial activities, Farmaco 57 (2002) 715–722, https://doi.org/10.1016/S0014-827X(02)01263-6.

[2] C.-B. Cui, H. Kakeya, G. Okada, R. Onose, H. Osada, Novel mammalian cell cycle inhibitors, tryprostatins A, B and other diketopiperazines produced by Aspergillus fumigatus. I. Taxonomy, fermentation, isolation and biological properties, J. Antibiot. 49 (1996) 527–533, https://doi.org/10.7164/antibiotics.49.527.

[3] T.H. Kang, K. Matsumoto, Y. Murakami, H. Takayama, M. Kitajima, N. Aimi, H. Watanabe, teropodine and isopteropodine positively modulate the function of rat muscarinic M (1) and 5-HT (2) receptors expressed in Xenopus oocyte, Eur. J. Pharmacol. 444 (2002) 39–45, https://doi.org/10.1016/S0014-2999(02)01608-4.

[4] E. Garcia Prado, M.D. Garcia Gimenez, R. De la Puerta Vazquez, J.L. Espartero Sanchez, M.T. Saenz Rodriguez, Antiproliferative effects of mitraphylline, a pentacyclic oxindole alkaloid of Uncaria tomentosa on human glioma and neuroblastoma cell lines, Phytomedicine 14 (2007) 280–284, https://doi.org/10.1016/j.phymed.2006.12.023.

[5] N. Arumugam, A.I. Almansour, R. Suresh Kumar, A.J.M. Ali Al-Aizari, S. Ibrahim Alaqeel, S. Kansız, V. Siva Krishna, D. Sriram, N. Dege, Regio- and diastereoselective synthesis of spiropyrroloquinoxaline grafted indole heterocyclic

hybrids and evaluation of their anti-Mycobacterium tuberculosis activity, RSC Adv 19 (2020) 23522–23531, https://doi.org/10.1039/D0RA02525A.
[6] Y. Huang, W. Min, Q.-W. Wu, J. Sun, D.-H. Shi, C.-G. Yan, Facile one-pot synthesis of spirooxindole-pyrrolidine derivatives and their antimicrobial and acetylcholinesterase inhibitory activities, New J. Chem. 42 (2018) 16211–16216, https://doi.org/10.1039/C8NJ03813A.
[7] E. Rajanarendar, S. Ramakrishna, K.G. Reddy, D. Nagaraju, Y.N. Reddy, A facile synthesis, anti-inflammatory and analgesic activity of isoxazolyl-2,3-dihydrospiro [benzo[f]isoindole-1,3′ -indoline]-2′,4,9-triones, Bioorg. Med. Chem. Lett. 23 (2013) 3954–3958, https://doi.org/10.1016/j.bmcl.2013.04.053.
[8] M.J. Kornet, A.P. Thio, Oxindole-3-spiropyrrolidines and -piperidines. Synthesis and local anesthetic activity, J. Med. Chem. 19 (1976) 892–898, https://doi.org/10.1016/j.bmcl.2013.04.053.
[9] N. Arumugam, A.I. Almansour, R. Suresh Kumar, D. Kotresha, R. Saiswaroop, S. Venketesh, Dispiropyrrolidinyl-piperidone embedded indeno[1,2-b]quinoxaline heterocyclic hybrids: synthesis, cholinesterase inhibitory activity and their molecular docking simulation, Bioorg. Med. Chem. 27 (2019) 2621–2628, https://doi.org/10.1016/j.bmc.2019.03.058.
[10] D.H. Nam, K.Y. Lee, C.S. Moon, Y.S. Lee, Synthesis and anticancer activity of chromone-based analogs of lavendustin A, Eur. J. Med. Chem. 45 (2010) 4288–4292, https://doi.org/10.1016/j.ejmech.2010.06.030.
[11] P. Valenti, A. Bisi, A. Rampa, F. Belluti, S. Gobbi, A. Zampiron, M. Carrara, Synthesis and biological activity of some rigid analogues of flavones-8-acetic acid, Bioorg. Med. Chem. 8 (2000) 239–246, https://doi.org/10.1016/S0968-0896(99)00282-5.
[12] L.C. Lin, Y.C. Kuo, C.J. Chou, Cytotoxic biflavonoids from Selaginella delicatula, J. Nat. Prod. 63 (2000) 627–630, https://doi.org/10.1021/np990538m.
[13] Y. Shi, T. Fukai, H. Sakagami, W. Chang, P. Yang, F. Wang, T. Nomura, Cytotoxic flavonoids with isoprenoid groups from morus mongolica, J. Nat. Prod. 64 (2001) 181–188, https://doi.org/10.1021/np000317c.
[14] R. Larget, B. Lockhart, P. Renard, M. Largeron, A convenient extension of the Wessly-Moser rearrangement for the synthesis of substituted alkylaminoflavones as neuroprotective agents in vitro, Bioorg. Med. Chem. Lett. 10 (2000) 835–838.
[15] A. Groweiss, J.H. Cardellins, M.R. Boyd, HIV-inhibitory prenylated xanthones and flavones from Maclura tinctoria, J. Nat. Prod. 63 (2000) 1537–1539, https://doi.org/10.1021/np000317c.
[16] H.R. Park, K. Park, Y. Chong, 2-Arylmethylaminomethyl-5,6-dihydroxychromone derivatives with selective anti-HCV activity, Bioorg. Med. Chem. Lett. 21 (2011) 3202–3205, https://doi.org/10.1016/j.bmcl.2011.04.055.
[17] T. Zhou, Q. Shi, C. Chen, H. Zhu, L. Huang, P. Ho, K. Lee, Anti-AIDS agents 79. Design, synthesis, molecular modelling and structure-activity relationships of novel dicamphanoyl-2′,2′-dimethyldihydropyranochromone (DCP) analogs as potent anti-HIV agents, Bioorg. Med. Chem. 18 (2010) 6678–6689, https://doi.org/10.1016/j.bmc.2010.07.065.
[18] Y. Deng, J.P. Lee, M. Tianasoa-Ramamonjy, J.K. Synder, S.A.D. Etages, D. Kanada, M.P. Synder, C.J. Turner, New antimicrobial flavones from Physena madagascariensis, J. Nat. Prod. 63 (2000) 1082–1089, https://doi.org/10.1021/np000054m.
[19] I.A. Khan, M.A. Avery, C.L. Burandt, D.K. Goins, J.R. Mikell, T.E. Nash, A. Azadega, L.A. Walker, Antigiardial activity of isoflavones from Dalbergia frutescens bark, J. Nat. Prod. 63 (2000) 1414–1416, https://doi.org/10.1021/np000010d.
[20] W.G. Ma, N. Fuzzati, S.L. Lu, D.S. Gu, K. Hostettmann, Further chromones from Eriosema tuberosum, Phytochemistry 43 (1996) 1339–1343, https://doi.org/10.1016/S0031-9422(96)00494-3.
[21] P. Pietta, Flavonoids as antioxidants, J. Nat. Prod. 63 (2000) 1035–1042, https://doi.org/10.1021/np9904509.
[22] P. Thanigaimalai, K. Lee, V.K. Sharma, J. Yun, Y. Kim, S. Jung, Design and synthesis of novel hydroxyalkylaminomethylchromones for their IL-5 inhibitory activity, Bioorg. Med. Chem. 18 (2010) 4625–4629, https://doi.org/10.1016/j.bmc.2010.05.028.
[23] R. Jiao, F. Xu, X. Huang, H. Li, W. Liu, H. Cao, L. Zang, Z. Li, H. Hua, D. Li, Antiproliferative chromone derivatives induce K562 cell death through endogenous and exogenous pathways, J. Enzyme Inhib. Med. Chem 35 (2020) 759–772, https://doi.org/10.1080/14756366.2020.1740696.
[24] J. Yue, S. Chen, X. Zuo, X.-L. Liu, S.-W. Xu, Y. Zhou, Diversity-oriented one-pot multicomponent synthesis of chromanone-based 3,3′-pyrrolidinyl-spirooxindoles via a 1,3-dipolar cycloaddition reaction, Tetrahedron Lett 60 (2019) 137–141, https://doi.org/10.1016/j.tetlet.2018.11.075.
[25] R. Vasudevan Sumesh, M. Muthu, A.I. Almansour, R. Suresh Kumar, N. Arumugam S. Athimoolam, E. Arockia Jeya Yasmi Prabha, R. Ranjith Kumar, Multicomponent Dipolar Cycloaddition Strategy: Combinatorial Synthesis of Novel Spiro-Tethered Pyrazolo[3,4- b]quinoline Hybrid Heterocycles, ACS Comb. Sci. 18 (2016) 262–270, https://doi.org/10.1021/acscombsci.6b00003.
[26] M.J. Turner, J.J. McKinnon, S.K. Wolff, D.J. Grimwood, P.R. Spackman, D. Jayatilaka, M.A. Spackman, Crystal Explorer, University of Western Australia, 2017, 17, http://hirshfeldsurface.net.
[27] M.J. Frisch, G.W. Trucks, H.B. Schlegel, G.E. Scuseria, M.A. Robb, J.R. Cheeseman, G. Scalmani, V. Barone, B. Mennucci, G.A. Petersson, *GAUSSIAN 09*; Revision A02, in: R. Dennington II, T. Keith, J. Millam (Eds.), *GaussView*; Version 4.1, Gaussian Inc., Wallingford, CT, USA, 2009. Semichem Inc.: Shawnee Mission, KS, USA, 2007.
[28] A.E. Reed, L.A. Curtiss, F. Weinhold, Intermolecular interactions from a natural bond orbital, donor-acceptor viewpoint, Chem. Rev. 88 (1988) 899–926, https://doi.org/10.1021/cr00088a005.
[29] K. Takao, M. Yamashita, A. Yashiro, Y. Sugita, Synthesis and Biological Evaluation of 3-Benzylidene-4-chromanone Derivatives as Free Radical Scavengers and α-Glucosidase Inhibitors, Chem. Pharm. Bull. 64 (2016) 1203–1207, https://doi.org/10.1248/cpb.c16-00327.
[30] N. Arumugam, A.I. Almansour, R. Suresh Kumar, S.M. Soliman, E. Viswanathan, K. Perumal, G. Angamuthu, P. Karuppiah, N.A. Al-Dhabi, Synthesis, structure and biological evaluation of highly functionalized 2-azetidinone integrated spirooxindolopyrrolidine heterocyclic hybrid, J. Mol. Struct. 1250 (2022), 131745, https://doi.org/10.1016/j.molstruc.2021.131745.
[31] N. Arumugam, A.I. Almansour, R. Suresh Kumar, S.M. Soliman, E. Viswanathan, N. Dege, P.Amaladas S.I.Alaqeel, K. Perumal, Stereoselective synthesis, structural determination, computational studies and antimicrobial activity of novel class of spiropyrroloquinoxaline engrafted ferrocenoindole hybrid heterocycle, J. Mol. Struct. 1252 (2022), 132131, https://doi.org/10.1016/j.molstruc.2021.132131.
[32] Crystallographic data (including structure factors) for the compounds **6** in this article have been deposited with the Cambridge Crystallographic Data Centreas supplementary publication number CCDC 2127283. Copies of the data can be obtained, free of charge, on application to CCDC, 12 Union Road, CambridgeCB2 1EZ, UK.
[33] S. Mathusalini, V. Viswanathan, P.S. Mohan, C.H. Lin, D. Velmurugan, D. Crystal structure of 4′-(2-methoxyquinolin-3-yl)-1′-methyldispiro [indan-2, 2′-pyrrolidine-3′, 3″-indoline]-1, 3, 2″-trione, Acta Crystallogr. E: Crystallogr. Commun. 71 (2015) o1038–o1039, https://doi.org/10.1107/S2056989015023026.
[34] M.A. Ali, R. Ismail, S.C. Tan, C.S. Yeap, H.K. Fun, 5, 6-Dimethoxy-4′, 5′-diphenylindane-2-spiro-3′-pyrrolidine-2′-spiro-3″-indoline-1, 2″-dione, Acta Crystallogr E: 66 (2010) o2533–o2534, https://doi.org/10.1107/S1600536810035865.
[35] V. Viswanathan, N.S. Rao, R. Raghunathan, D. Velmurugan, Crystal structures of two substituted thiazolidine derivatives, Acta Crystallogr E: Crystallogr. Commun. 72 (2016) 1126–1129, https://doi.org/10.1107/S2056989016011336.
[36] N. Sivakumar, V. Viswanathan, J.N.S. Rao, R. Raghunathan, D. Velmurugan, Crystal structure of 6-(4-chlorophenyl)-6a-nitro-6, 6a, 6b, 7, 9, 11a-hexahydrospiro [chromeno [3′, 4′: 3, 4] pyrrolo [1, 2-c] thiazole-11, 11′-indeno [1, 2-b] quinoxaline] chloroform monosolvate, Acta Crystallogr. E: Structure Reports Online 70 (2014) o1111–o1112, https://doi.org/10.1107/S1600536814020601.
[37] S. Syed Abuthahir, M. Nizam Mohideen, V. Viswanathan, D. Velmurugan, J. Nagasivarao, The crystal structures of 6′-(4-chlorophenyl)-and 6′-(4-methoxyphenyl)-6a′-nitro-6a′, 6b′, 7′, 9′, 10′, 12a′-hexahydro-2H, 6′ H, 8′ H-spiro [acenaphthylene-1, 12′-chromeno [3, 4-a] indolizin]-2-one, Acta Crystallogr. E: Crystallogr. Commun. 75 (2019) 218–222, https://doi.org/10.1107/S2056989019000422.
[38] S. Syed Abuthahir, M. Nizam Mohideen, V. Viswanathan, D. Velmurugan, J. Nagasivarao, Crystal structure of 6-(4-chlorophenyl)-6a-nitro-6a, 6b, 8, 9, 10, 12a-hexahydro-6H, 7H-spiro [chromeno [3, 4-a] indolizine-12, 11′-indeno [1, 2-b] quinoxaline], Acta Crystallogr. E: Crystallogr. Commun. 75 (2019) 255–259, https://doi.org/10.1107/S2056989019000975.
[39] V. Viswanathan, J.N.S. Rao, R. Raghunathan, D. Velmurugan, Crystal structures of two triazola-dioxola-benzenacyclononaphanes, Acta Crystallogr. E: Crystallogr. Commun. 71 (2015) 827–831, https://doi.org/10.1107/S205698901501141X.
[40] A.M. Moustafa, A.S. Girgis, S.M. Shalaby, E.R. Tiekink, 1′-Methyl-4′-(4-methylphenyl) dispiro [indane-2, 3′-pyrrolidine-2′, 3″-indoline]-1, 2″-dione, Acta Crystallogr E 68 (2012) o2197–o2198, https://doi.org/10.1107/S1600536812028012.
[41] D.T. Cremer, J.A. Pople, General definition of ring puckering coordinates, J. Am. Chem. Soc. 97 (1975) 1354–1358, https://doi.org/10.1021/ja00839a011.
[42] R. Chang, Chemistry, 7th ed., McGraw-Hill, New York, NY, USA, 2001.
[43] B. Kosar, C. Albayrak, Spectroscopic investigations and quantum chemical computational study of (E)-4-methoxy-2-[(p-tolylimino) methyl] phenol, Spectrochim. Acta 78 (2011) 160–167, https://doi.org/10.1016/j.saa.2010.09.016.
[44] T.A. Koopmans, Über die Zuordnung von Wellenfunktionen und Eigenwerten zu den Einzelnen Elektronen Eines Atoms, Physica 1 (1933) 104–113, https://doi.org/10.1016/S0031-8914(34)90011-2.
[45] R.G. Parr, W. Yang, Density-Functional Theory of Atoms and Molecules, Oxford University Press, New York, NY, USA, 1989.
[46] R.G. Parr, L.V. Szentpaly, S. Liu, Electrophilicity index, J. Am. Chem. Soc. 121 (1999) 1922–1924, https://doi.org/10.1021/ja983494x.
[47] R.N. Singh, A. Kumar, R.K. Tiwari, P. Rawat, V.P. Gupta, A combined experimental and quantum chemical (DFT and AIM) study on molecular structure, spectroscopic properties, NBO and multiple interaction analysis in a novel ethyl 4-[2-(carbamoyl) hydrazinylidene]-3, 5-dimethyl-1H-pyrrole-2-carboxylate and its dimer, J. Mol. Strut. 1035 (2013) 427–440, https://doi.org/10.1016/j.molstruc.2012.11.059.
[48] I.Hubert Joe, I. Kostova, C. Ravikumar, M. Amalanathan, S.C. Pinzaru, Theoretical and vibrational spectral investigation of sodium salt of acenocoumarol, J. Raman Spectrosc. 40 (2009) 1033–1038, https://doi.org/10.1002/jrs.2226.
[49] S. Sebastian, N. Sundaraganesan, The spectroscopic (FT-IR, FT-IR gas phase, FT-Raman and UV) and NBO analysis of 4-Hydroxypiperidine by density functional method, Spectrochim. Acta Part A Mol. Biomol. Spectrosc. 75 (2010) 941–952, https://doi.org/10.1016/j.saa.2009.11.030.